Journal of Environmental Chemical Engineering 12 (2024) 114572

Contents lists available at ScienceDirect

Journal of Environmental Chemical Engineering

journal homepage: www.elsevier.com/locate/jece

Revealing the role of individual components in the high performance photocatalytic mineralization of mixtures of organohalogen pollutants

Carmen Barquín, María J. Rivero, Inmaculada Ortiz *

Departamento de Ingenierías Química y Biomolecular, Universidad de Cantabria, Avda. Los Castros, s/n, Santander 39005, Spain

ARTICLE INFO

Keywords:
Water remediation
Photocatalyst performance
Organohalogen compounds
Mineralization kinetics
Halogen ions release

ABSTRACT

In this work, we address the photocatalytic mineralization of single-component solutions and mixtures of three organohalogenated compounds, dexamethasone (DEX), S-metolachlor (MTLC) and dichloroacetic acid (DCA) using a low-cost TiO_2/rGO composite. A detailed experimental analysis has evidenced the positive influence of the presence of DCA on the degradation, and mineralization kinetics, as well as on the release of ions into solution, which is explained by the acidic pH of the solutions containing this compound. Mineralization curves of the aqueous mixtures follow two distinct kinetic trends, the first is assigned to the breakdown of the primary compounds and proceeds with second order kinetics ($k = 0.58 \times 10^{-3}$ mM^{-1} min^{-1} at neutral pH, and $k = 1.19 \times 10^{-3}$ mM^{-1} min^{-1} at pH 4 and the tertiary mixture). In the second zone, which progresses at a slower rate and is attributed to the mineralization of intermediate compounds, all mixtures have kinetic constants within the range $(9.7 \pm 0.7) \times 10^{-3}$ min^{-1}. The progress in the release of halogen ions (F^- and Cl^-) and NH_4^+, together with the changes in the chemical composition of the catalyst determined by XPS, allow to conclude that no organohalogenated intermediates remain in solution after treatment. Furthermore, the lack of phytotoxicity of the treated mixtures is confirmed with germination indices (GI), reaching GI values above the control point for the time of complete mineralization; this together with the stability of the catalyst after 5 reuse cycles highlights the green and sustainable nature of the selected photocatalytic remediation process.

1. Introduction

Water remediation has become a priority to meet the global need for clean water. Therefore, it is necessary to develop efficient and cost-effective alternatives that are capable of degrading contaminants of emerging concern (CECs) and other pollutants in wastewater treatment plants [1–3]. Among the various groups of CECs, organohalogen compounds (OHXs) are of global concern due to their persistence in water and the potential for adverse effects on the eco-environment and human health [4–6]. In this context, photocatalysis, and more specifically heterogeneous photocatalysis, emerges as a process involving the frontiers of environmental science and technology, that offers good prospects for a cleaner, healthier, and more resilient planet [7–12]. Photocatalysis is based on the promotion of electrons from the valence band to the conduction band through the illumination of a semiconductor with photons of energy equal to or greater than its energy gap [13]. Photocatalytic processes have aroused great interest among the scientific community, as supported by the nearly 4000 articles listed in the Web of Science database since 2020 using the keywords "photocatalysis", "water" and "remediation". TiO_2 is the most widely used semiconductor in heterogeneous photocatalysis, whose generated radicals react with most organic compounds, [3,14,15]. However, it has the disadvantage of rapid recombination of photogenerated electron-hole pairs, leading to its rapid deactivation [16–20]. Therefore, much effort has been put into the synthesis and characterization of new materials outperforming the activity of TiO_2 [21–35]. Among the most recent contributions to the synthesis of new catalytic materials, we can mention the successful synthesis of a Cu-ZnO/g-C_3N_4 composite with enhanced photocatalytic activity, capable of efficiently degrading several antibiotics under visible light irradiation [36], the superior performance in the degradation of the herbicide glyphosate with a metal-organic framework (MOF) based on scandium [37], or the higher degradation activity of perfluorooctanoic acid reported with boron nitride, mainly due to its greater surface hydrophobicity [38].

Another line of research that has received a great deal of attention focuses on the development of new reactor configurations [39–46]. Although several works have reached the pilot plant scale, the technology has not yet reached real plant implementation, because of the

---

* Corresponding author.
E-mail address: ortizi@unican.es (I. Ortiz).

https://doi.org/10.1016/j.jece.2024.114572
Received 30 July 2024; Received in revised form 14 October 2024; Accepted 24 October 2024

higher residence time, and consequently, equipment size, needed for the remediation of water when compared to more established alternatives as recently reported by Rengifo-Herrera and Pulgarin [47] and by Kuspanov et al. [48]. Knowing what variables affect the performance of the catalytic process and quantifying their kinetic influence is essential to make progress in this direction. A holistic approach that considers the photocatalytic performance as a function of both the characteristics of the material and the liquid medium as well as their change over time, is the best way to develop kinetic models capable of predicting the behavior of the system with the treatment time, and to advance in the correct process design and optimization.

This work aims to create new knowledge that helps understand the influence of the variables that affect the kinetic performance of the photocatalyst in water remediation. With this purpose we have focused the work on the degradation and mineralization of waters containing three organohalogen compounds, OHXs, representative of common anthropogenic activities. Therefore, we have selected 1) fluorinated dexamethasone (DEX), a synthetic glucocorticoid with high anti-inflammatory effect that has been detected in surface waters, drinking water or wastewaters [49,50], 2) chlorinated S-metolachlor (MTLC), which belongs to the chemical group of chloroacetanilides and is a broad-spectrum herbicide [51,52], and 3) double-chlorinated dichloroacetic acid (DCA), which is an haloacetic acid with highly stable polar molecules, formed usually during water disinfection processes [5,53]. The chemical stability of the C-halogen bonds makes these contaminants recalcitrant to conventional water treatment processes [4]. Halogens are more electronegative than carbons, resulting in a C-halogen bond that is polarized; the carbon atom has a partial positive charge while the halogen atom has a partial negative charge [54].

The assessment of the effectiveness of new technologies for water remediation goes beyond monitoring the degradation of primary contaminants and must comply with regulated quality standards based on the end use; according to the Regulation (EU) 2020/741 on minimum requirements for water reuse, and specifically in Spain, it is mandatory to comply with Royal Decree 1620/2007, which establishes the legal regime for the reuse of treated water. In this context, the change in the dissolved organic carbon or the toxicity of the aqueous medium after treatment, are essential parameters to evaluate the remediation process. Besides, in the case of OHXs, the release of halogen ions from the breakdown of the organic molecules must also be contemplated.

In our work, we provide essential information for the design of photocatalytic degradation of OHXs in water remediation. Specifically, we conduct a kinetic analysis after applying a thorough methodology that allows us to identify the conditions and degradation rates of the primary pollutants, as well as those of the intermediate compounds formed during degradation. In light of the significance of comprehensive mineralization of organic compounds, we examine the evolution of global parameters over time in conjunction with the ions released upon the disruption of organic molecules. Our approach offers a comprehensive rationale for the observed outcomes through an integrated analysis of the changes in the properties of the aqueous medium and the catalytic material. Moreover, the methodology presented in this work can be extended to diverse applications in water remediation, facilitating advancements, scale-up, and optimization of photocatalytic degradation processes. With this purpose, a detailed experimental plan has been followed using a low-cost and easily synthesized TiO_2/rGO composite, with improved efficiency in charge separation over TiO_2, and comparing its performance in the degradation and mineralization of single-compound solutions, binary and tertiary mixtures of the selected OHXs. Furthermore, the release of halogen ions to the solution, structural and morphological changes of the photocatalyst and the change in phytotoxicity over time has been determined. The results and methodology developed here are essential for process design and scale-up.

2. Experimental

2.1. Materials

The model OHXs pollutants DEX ($C_{22}H_{29}FO_5$) and MTLC ($C_{15}H_{22}ClNO_2$) PESTANAL® are purchased from Sigma-Aldrich, while DCA ($C_2H_2Cl_2O_2$) is purchased from Acros Organics. For the TiO_2/rGO synthesis, TiO_2 Aeroxide® P25 is provided by Evonik Degussa and graphene oxide (GO) water dispersion 4 mg mL^{-1} is acquired from Graphenea. Nitric acid (HNO_3) 65 % (v/v) EMSURE® is purchased from Sigma Aldrich and used for pH adjustment. Experiments are performed with ultrapure (UP) water (Milli-Q Millipore system, 18.2 MΩ cm at 25 °C). Samples are filtered through 0.45 μm polypropylene syringe filters from Agilent Technologies prior to analytical determination. All reagents and materials are of analytical grade and have been used without further treatment.

2.2. Synthesis of the composite

TiO_2/rGO photocatalyst containing 5 % wt. of graphene oxide, has been synthesized hydrothermally by a facile and sustainable method. In a typical synthesis procedure, 10 mL of GO water dispersion are diluted in 100 mL of ultrapure water. Further, 0.76 g of commercial TiO_2 are added to the reaction mixture and stirring for 60 min. The reaction mixture is then transferred to a 150 mL Teflon autoclave reactor with stainless steel housing and heated at 120 °C for 180 min. Finally, the resulting TiO_2/rGO composite is dried in an oven at 80 °C. Further information is outlined in a prior publication [55].

2.3. Photocatalyst characterization

The morphology of the catalyst is examined by Transmission Electron Microscopy (TEM) in a JEOL JEM-1011 HR equipment at an applied voltage of 80 kV.

The catalyst surface is characterized by X-ray photoelectron spectroscopy (XPS, Physical Electronics model 5700 C) with Mg Kα radiation (1253.6 eV). The maximum of the C1s peak is set to 284.5 eV and used as reference for shifting the whole spectrum, corresponding to surface adventitious carbon.

Electrochemical properties are determined using Electrochemical Impedance Spectroscopy (EIS) measurements, at constant voltage of −0.8 V (vs. Ag/AgCl) and frequency ranging between 10 kHz and 0.1 Hz. For that purpose, the preparation of a photoanode is needed, with a geometric area of 10 cm^2 and Toray carbon paper treated with PTFE as support. Ink formulation using isopropanol as solvent and Nafion D521 as binder, with a catalyst/binder ratio of 70/30 wt% has been used [56,57]. The ink is placed in ultrasound equipment prior to its use. The ink is sprayed onto the substrate on a heating plate at 70 °C using an airbrush. EIS measurements have been carried out in an adapted cell under UV-A LED light (100 mW cm^{-2}), previously described [56,57].

BET surface area is determined from N_2 adsorption-desorption isotherms at 77 K, measured in an ASAP 2420 Micromeritics. The isotherms are obtained in the range of relative pressures from 0.01 to 1. The BET equation for determining the surface area of materials is applicable in the range of relative pressures up to 0.4.

Characterization techniques have been applied to the catalyst samples before and after use. Further characterization of the composite TiO_2/rGO can be found in previous works [55,58].

2.4. Photocatalytic activity

For the evaluation of the photocatalytic activity, synthetic solutions of single-component, binary and tertiary mixtures have been prepared, with 0.11 mM of each OHX in all of them; equivalent to 43 mg L^{-1} of DEX, 30 mg L^{-1} of MTLC, and 14 mg L^{-1} of DCA. DEX, MTLC and DCA single solutions have initial DOC values of 2.42 mM of carbon (C) (29.04 mg L^{-1}), 1.65 mM C (19.80 mg L^{-1}), and 0.22 mM C (2.64 mg L^{-1}), respectively. The initial DOC value of the binary mixture DEX + MTLC is 4.07 mM C (48.84 mg L^{-1}), while the initial DOC value of the tertiary mixture is 4.29 mM C (51.48 mg L^{-1}). Based on previous results of the research group [55,59,60], a catalyst concentration of 0.5 g L^{-1} of TiO_2/rGO has been used in all experiments. The experiments are conducted in an open photoreactor with continuous stirring, operating under ambient pressure and temperature conditions. The setup consists of a 1 L Pyrex glass reactor equipped with UV-A LED lights purchased from APRIA SYSTEMS, emitting at fixed 365 nm wavelength. The photoreactor housing is equipped with 30 LEDs, organized in 10 rows and placed at a distance of 1.5 cm from the reactor. For the sampling procedure, the photoreactor is equipped with a lid that can be removed momentarily. Once the adsorption period is completed, the solutions are illuminated with an average irradiance of 200 W m^{-2}. Samples are collected at predefined times, filtered through 0.45 μm, and subjected to analysis. When necessary, the pH is adjusted with nitric acid 65 % (v/v). Both DEX and MTLC are quantified in a high-performance liquid chromatograph (HPLC) from Agilent, Series 1100, with detection limits of 1.27×10^{-4} and 3.52×10^{-4} mM, respectively. The HPLC is equipped with an Agilent Zorbax 80 Å Extend-C18 column (5 μm, 3.0 × 150 mm) coupled to a diode array detector (1260 DAD-HS). The injection volume is 50 μL, and the column temperature is maintained at 30 °C. Acetonitrile and ultrapure water are employed as mobile phases for both compounds, in isocratic mode. For DEX and MTLC, the ratios between mobile phases are 40/60 and 60/40 (v/v), with flow rates of 0.5 mL and 0.7 mL min^{-1}, respectively. The retention times for DEX and MTLC are 3.0 min and 3.8 min, respectively, with selected wavelengths of 240 nm and 214 nm, respectively.

DCA concentration and the released Cl^-, F^-, and NH_4^+ ions to the solution are determined in a Dionex ICS-5000 ion chromatograph, equipped with autosampler. The instrument has a dual pump that allows the measurement of both anions and cations. Dionex Chromeleon™ v.6.80 is the used software. IonPac AS9-HC (4.0 × 50 mm) anionic column, and IonPac CS-12A (4.0 × 250 mm) cationic column are used, both commercialized by Thermo Scientific. The mobile phases are Na_2CO_3 9 mM for the anionic column and methanesulfonic acid (MSA) 18 mM for the cationic column, both with a flow rate of 1.0 mL min^{-1} in isocratic mode, and a pressure of approximately 1200 and 1000 psi, respectively. Under these conditions, the retention time of DCA is 10.2 min and the detection limit for DCA is 7.75×10^{-3} mM. The retention times for F^-, Cl^- and NH_4^+ are 4.35 min, 6.48 min and 5.80 min, respectively. The detection limit of fluoride is 2.63×10^{-3} mM, of chloride 1.41×10^{-3} mM and of ammonium 5.55×10^{-3} mM. Measurements of dissolved organic carbon (DOC) are carried out to determine the degree of mineralization in a Shimadzu TOC-V-CPH analyser with autosampler (ASI-V) and DOC detection limit of 0.16 mM.

Each experiment is conducted twice to increase accuracy. The error bars depicted in the figures represent the standard deviation of the duplicates, expressed in dimensionless units. The pH values are monitored throughout the experiments using a Hanna Edge pH meter. In the reusability experiments, stirring of the solution stops after each cycle and the catalyst particles settle in the reactor. The aqueous phase is removed after each cycle with a syringe, the catalyst is left in the reactor, and a fresh solution is added to start the next cycle, keeping the rest of operating conditions constant. At the end of the 5 reusability runs, when the TiO_2/rGO particles settle in the bottom of the reactor, most of the aqueous phase is removed, and the particles are transferred to a beaker where they are dried in an oven at 100 °C and the final mass recovered can be weighed. Knowing the value of the final mass, it is assumed that the mass lost in each cycle is the same. To avoid the influence of the mass loss due to the sampling procedures in the cycles, a performance factor is used to express the kinetic constants. The performance factor is calculated as the quotient between the kinetic constant and the initial mass of catalyst in each cycle. The final mass after the 5 cycles is weighed and the mass loss is assumed to be equal in each cycle.

The kinetic parameters of degradation, mineralization and halogen ions release in the experiments are estimated using the simulation software Aspen Custom Modeler V.14. The values are obtained with the estimation tool of the Aspen software, following the least squared error criterion, with a maximum of 1150 iterations and a solution convergence tolerance of 0.0001. The input data for the software are the experimental concentration values. To estimate the values of kinetic constants, the software uses a first/second order kinetic model, as appropriate. For each experimental point, the standard deviation, σ, is calculated with its corresponding simulated value in Aspen. Global values of standard deviation are calculated as the average of the standard deviations in each experiment.

In the mixtures, DEX and MTLC data fit perfectly to a second order kinetic equation, as shown in Eq. 1.

$$\frac{dC}{dt} = -k \cdot C_{DEX} \cdot C_{MTLC} \tag{1}$$

where C is the OHX concentration (mM), C_{DEX} is the experimental DEX concentration (mM), C_{MTLC} is the experimental MTLC concentration (mM) for a given time, and k is the kinetic constant (mM^{-1} min^{-1}).

2.5. Phytotoxicity assessment

The toxicity of the samples is assessed using the Phytotestkit microbiotest supplied by MicroBio Tests Inc. These tests, which conform to ISO standard 18763, allow the assessment of seed germination and plant growth for the specie *Sorghum saccharatum* (SOS). The procedure involves germination of seeds by adding 20 mL of the pre-filtered sample to the test plates, followed by a growth period of 72 h at a temperature of 25 °C. Comparative control tests are also carried out using 20 mL of ultrapure water. The number of germinated seeds is then determined at the beginning, middle and end of the photocatalytic treatment, together with root and shoot measurements. The results are processed using ImageJ software, version 1.54d. The seed is considered germinated if it exhibits a root or shoot length exceeding 1 mm. Based on these values, the Germination Index (GI) is calculated using the Eq. 2, according to the procedures described by Batista et al. [61].

$$IG(\%) = \frac{RSG \cdot RRG}{\overline{RSG} \cdot \overline{RRG}} \cdot 100 \tag{2}$$

where RSG is the number of germinated seeds in the sample plate, RRG is the root growth in the sample plate, $\overline{RSG}$ is the average of germinated seeds in the control, and $\overline{RRG}$ is the average root or shoot growth in the control plates. GI is calculated at the beginning, middle and end of the photocatalytic treatment for each cycle. The shown GI values are the average of all the cycles.

3. Results and discussion

3.1. Degradation and mineralization kinetics of the selected OHXs

The photocatalytic degradation of aqueous mixtures of the organohalogen compounds, DEX, MTLC and DCA, is carried out with the easily synthesized TiO_2/rGO photocatalyst under UV-A light. Fig. 1 shows the change in the concentration of the selected OHXs in single-component solutions (a), binary (b) and tertiary (c) mixtures. Experiments are carried out keeping the initial conditions of the aqueous solutions, no pH control, in the attempt to simplify water remediation processes. Before turning on the lamps, the solutions are kept in the dark for 30 min to allow adsorption of the pollutants on the catalyst. MTLC is the compound that shows higher adsorption on the TiO_2/rGO photocatalyst, decreasing from 50 % of its initial concentration in single-component solutions [58] to 20 % and 10 % in binary and tertiary mixtures, respectively. This phenomenon occurs because when more than one

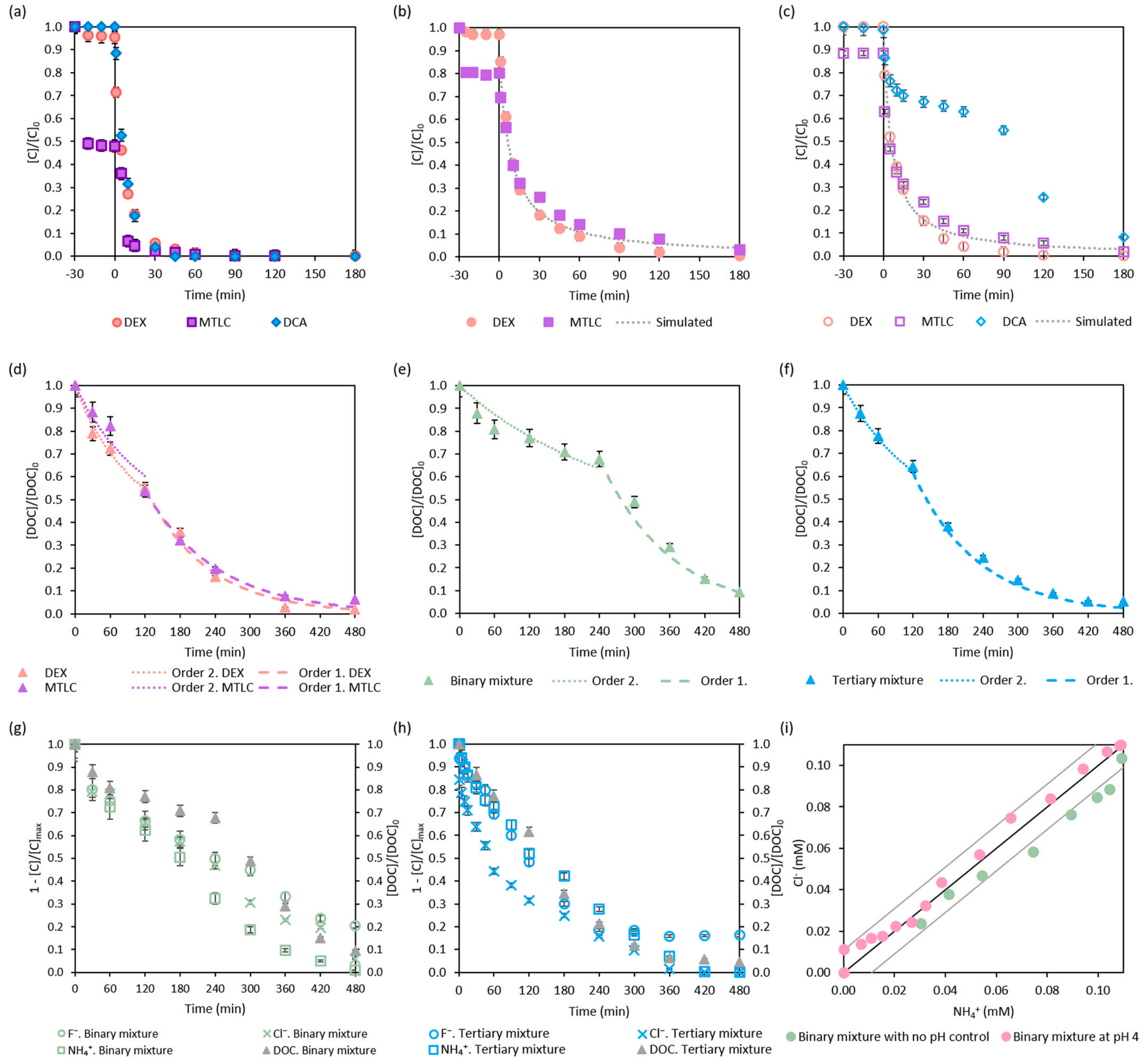

Fig. 1. Photocatalytic degradation of DEX, MTLC and DCA in (a) single-component solutions, (b) binary and (c) tertiary mixtures after 180 min of irradiation with UV-A source at 365 nm with no pH control. Mineralization of DEX, MTLC and DCA in (d) single-component solutions, (e) binary and (f) tertiary mixtures after 480 min of irradiation with UV-A source at 365 nm with no pH control. Ions released expressed as 1 - the dimensionless measured concentration during the photocatalytic degradation of (g) binary and (h) tertiary mixtures with no pH control. Mass balance of chloride release and ammonia release in binary DEX + MTLC solutions for experiments with no pH control and pH 4 (i).

organic compound is in solution, the available catalyst is shared by all of them. In our work, the presence of DEX and DCA in the mixtures results in fewer adsorbed MTLC molecules because they are pushed away from the catalyst surface. With respect to DEX and DCA, there is no evidence of significant adsorption either in experiments with a single component or in mixtures, Fig. 1a-c [58,62]. In previous studies conducted by the research group, the degradation of these pollutants was evaluated using only photolysis. Neither MTLC nor DCA are susceptible to be degraded by photolysis. In the absence of catalyst, only a slight degradation occurs, with less than 10 % degradation after 330 min of UV-A irradiation. DEX is degraded by photolysis with UV-A light, with a pseudo-first order kinetic constant of 2.3 × 10^{-2} min^{-1}. Furthermore, the DEX removal rate increases by a factor of more than five with the addition of the photocatalyst [55,58,59].

The analysis of the kinetics of photocatalysis shows that, in single-component solutions, Fig. 1a, the data of the three components fit to a pseudo-first order kinetic model with kinetic constants of 12.8 × 10^{-2} min^{-1}, 16.4 × 10^{-2} min^{-1} and 12.3 × 10^{-2} min^{-1}, for DEX, MTLC and DCA, respectively. Fig. 1b-c displays the kinetic trends of the data of binary solutions DEX + MTLC, and tertiary solutions containing DCA. In addition to the influence of the presence of DEX on the lower adsorption of MTLC, a change in the kinetic trend is also observed. The data of DEX and MTLC shown in Fig. 1b have been fitted to a second order kinetic equation, Eq. 1, with an average constant of 1.20 mM^{-1} min^{-1} for binary solutions. This may indicate that when there is more than one degradable OHX, the photocatalytic sites of the catalyst are shared between both compounds.

Fig. 1c displays the kinetic data of the components in the tertiary mixture. Both DEX and MTLC fit to a second order equation with kinetic constant of 1.59 mM^{-1} min^{-1} that is slightly higher than in the binary mixture. What is surprising is that the presence of the third component, DCA, not only does not delay the degradation of the other two components, but has a positive effect on it. With respect to the change in DCA concentration, although it follows a pseudo-first order kinetic equation in single-component degradation, its degradation in the tertiary mixture is influenced by the presence of the other compounds, showing an S-shaped trend with two kinetic zones and an inflection point at times when more than 90 % of the other two components has been degraded; this points to a more effective degradation of DEX and MTLC with respect to DCA in the tertiary mixture.

One of the challenges in photocatalysis is to identify photocatalysts that can enhance reaction rates. In this study, we select the binary catalyst TiO_2/rGO because it yields significantly improved results compared to commercial TiO_2 alone. In summary, the composite significantly enhances the degradation kinetics of organohalogen compounds because of the optimized charge transfer within the catalyst. The primary reactive oxygen species (ROS) responsible for the observed degradation are hydroxyl radicals; but also, the TiO_2/rGO catalyst enhances the activity of superoxide radicals [55]. Also, regarding DEX degradation, bare TiO_2 is unable to degrade the molecules within the 120 minutes of light exposure, and halogenated compounds remain after treatment. This behavior was not observed with the TiO_2/rGO composite [58].

The degree of mineralization is one of the most significant parameters in water remediation of organic pollutants together with the change in toxicity. Fig. 1 shows the photocatalytic trend of DOC in single solutions of DEX and MTLC (d), the binary mixture of DEX and MTLC (e) and the tertiary mixture of DEX, MTLC and DCA (f) in experiments carried out with no pH control. In this work, the progress in DOC is supplemented with the analysis of the halogen and nitrogen ions released to the medium, Fig. 1g-h, with the data of the binary and tertiary mixtures, respectively.

The mineralization rates of DEX and MTLC single solutions are quite similar, with both curves exhibiting a similar trend. Two kinetic zones are appreciated; the first one that goes down to 30 %-40 % of the initial DOC corresponds to mineralization of the primary OHX, and the second zone corresponds to the mineralization of the intermediate compounds formed during the photocatalytic reaction pathways. Figure S1 in the supplementary material (SM) show the presence of intermediate compounds with the degradation time for binary mixtures determined by high-performance liquid chromatography (HPLC).

The mineralization of solutions with only DCA can not be monitored because the molecule has only two carbon atoms and the initial concentration of DOC is close to the detection limit of the analytical technique for the experimental conditions.

For the binary mixture, the presence of both kinetic zones is more pronounced and the rate of mineralization is lower. In all the analyzed cases, the first zone fits to a second order kinetic equation, whereas in the second zone the curves fit to a first order kinetic model. The values of the different kinetic constants are collected in Table 1. The second order kinetic constant in the binary mixture when the degradation takes place with no pH control is 0.58×10^{-3} mM^{-1} min^{-1}, being much lower than the values for single component solutions. This fact, is easily attributable to the higher carbon load present in the binary mixture in comparison with DEX and MTLC single-componet experiments. However, surprisingly, the binary mixture requires 1.3 longer times to reach 90 % mineralization than the tertiary mixture; being DCA a strong acidic compound, its presence in tertiary mixtures promotes the decrease in the initial pH, phenomenon that could be responsible for the enhanced mineralization kinetics.

3.2. Release of halogen and nitrogen ions

Giving that the DEX molecule has 1 atom of F, MTLC, 1 atom of Cl and 1 atom of N, and DCA 2 atoms of Cl, the change in the concentration of F^-, Cl^-, NO_2^-/NO_3^- and NH_4^+ has been monitored over time in the photocatalytic degradation of binary and tertiary mixtures, Fig. 1g-h. Since the MTLC molecule contains the nitrogen atom, the potential presence of nitrates and/or nitrites is investigated by ion chromatography. However, none of these ions has been detected. Nevertheless, it is found that the nitrogen atom is released in the form of ammonium, as previously reported by Vieira et al. [63].

Fig. 1g-h represent the ions released to the aqueous solution expressed as the difference between the concentration in the initial OHX and the measured concentration at a given time in dimensionless units, together with the change in the dissolved organic carbon in the corresponding mixture. Fig. 1g displays the ions evolution in the binary mixture. Here, the three ions follow the same trend with two kinetic zones, similar to the behavior observed for the dissolved organic carbon. This may indicate that the ions in the first zone correspond to the breakdown of the primary OHXs, whereas the second zone corresponds to the release of ions from the breakdown of intermediate compounds formed during the photocatalytic process. Fig. 1h displays the data corresponding to the tertiary mixture; the comparison between the two graphs (Fig. 1g-h) highlights the enhanced kinetics in the latter. The values of kinetic constants obtained with the Aspen estimation tool are collected in Table 2. Furthermore, all curves fall to zero for the final time of the experiments, except the curves corresponding to fluoride ions which are released about 80 % of the initial F concentration in DEX molecules. It has been previously evidenced that fluoride ions in aqueous solutions may be adsorbed on the photocatalyst surface simultaneously to their release until the solid becomes saturated [58].

Table 1
Kinetic constants for the photocatalytic degradation and mineralization of OHXs mixtures. BM: binary mixture. TM: tertiaty mixture.

Experiment	Degradation		Mineralization			
	Second order k (mM^{-1} min^{-1})	σ (mM)	First zone (0–120 min) Second order k (mM^{-1} min^{-1})	σ (mM)	Second zone (120–480 min) First order k (min^{-1})	σ (mM)
BM no pH control	1.20	4.23×10^{-3}	* 0.58×10^{-3}	6.64×10^{-2}	* 10.4×10^{-3}	1.82×10^{-2}
TM no pH control	1.59	4.22×10^{-3}	1.19×10^{-3}	9.75×10^{-3}	9.00×10^{-3}	2.82×10^{-2}
BM pH 4	1.55	4.43×10^{-3}	1.19×10^{-3}	4.76×10^{-2}	10.4×10^{-3}	4.63×10^{-2}
DEX no pH control	n.a.		2.81×10^{-3}	2.48×10^{-2}	9.47×10^{-3}	3.31×10^{-2}
MTLC no pH control	n.a.		3.70×10^{-3}	4.16×10^{-2}	8.13×10^{-3}	2.39×10^{-2}

n.a.: not applicable.
*The change in the mineralization kinetics for the binary mixture with no pH control took place after 240 min.

Table 2
Kinetic constants for the ions release and mineralization of the binary mixtures at different pH values.

Experiment	Ion release			
	First zone (0–120 min) Second order k (mM^{-1} min^{-1})	σ (mM)	Second zone (120–480 min) First order k (min^{-1})	σ (mM)
Binary mixture no pH control	4.84×10^{-2}	2.38×10^{-3}	4.24×10^{-3}	8.05×10^{-3}
Binary mixture pH 4	7.35×10^{-2}	2.71×10^{-3}	7.77×10^{-3}	2.87×10^{-3}

Being fluorine the more electronegative halogen [54], once the C-F bond is broken during the photocatalytic process, the negatively charged fluoride is attracted by electrostatic interactions to the carbonaceous compound of the TiO_2/rGO [64]. In a previous work we evaluated the zeta potential of the composite TiO_2/rGO, and the obtained isoelectric point was approximately 5.8 [55]. This indicates that at pH values below 5.8 the photocatalyst is positively charged; and this would explain the unbalance in the concentration of fluoride between the initial molecule and the final solution. Breakage of MTLC and its intermediate compounds would release Cl^- and NH_4^+ ions. Furthermore, Fig. 1i displays the good match between the concentration of Cl^- and NH_4^+. Grey lines in Fig. 1i represent the zone with ±10 % error around the bisector.

Giving that DCA is a strong acidic component whose presence lowers the pH value, the influence of this variable is analyzed; for this purpose, experiments of the degradation and mineralization of the binary mixture are carried out, setting the initial pH at a value of 4, which is the pH obtained in the tertiary mixture after the adsorption period. The results of degradation, mineralization and ions release of the binary mixture at pH 4 are displayed in Fig. 2a-b.

Although lowering the initial pH has no influence on the adsorption behavior of the OHXs on the photocatalyst (20 % adsorption of MTLC), the degradation and mineralization kinetics in the binary mixture are positively affected. As shown in Fig. 2a, the kinetic data of pollutants degradation fit to a second order model with a kinetic constant of 1.55 mM^{-1} min^{-1}, Table 1, value that is ≈1.3 times higher than the value with no pH control. Moreover, the comparison between the kinetic constants in the binary mixture at pH 4 and the tertiary mixture shows similar values, thereby reinforcing the conclusion that the pH of the solution exerts the strongest influence on the degradation rate of the pollutants.

Fig. 2b displays the results of the mineralization kinetics in the binary mixture with an initial pH of 4, together with the trend in the release of ions. The four curves follow a similar path with two differentiated zones that, as mentioned before, correspond to the degradation of the primary OHXs and of intermediate compounds, respectively. Kinetic constants for the release of ions are collected in Table 2. Up to 120 min (almost complete removal of the primary OHXs), the curves follow a second order kinetic model, with a kinetic constant value of 7.35×10^{-2} mM^{-1} min^{-1}. From 120–480 min, the concentration of ions fits to a first order kinetic model, with a kinetic constant value of 7.77×10^{-3} min^{-1}. These values are 1.5 and 1.8 times greater than the kinetic constant values obtained for the experiments with no pH control, which again suggests that a more acidic aqueous medium accelerates substantially the ions release. Although there is a decrease of the pH of the aqueous medium along the photocatalytic run, the presence of DCA keeps the pH value below 4.0 since the beginning of the experiment, Fig. 2c, improving the kinetics of DEX and MTLC degradation and mineralization. These results suggest that the attraction between F^- and Cl^- anions and the protons in the solution is more pronounced than the electrostatic forces between the fluorides and the catalyst surface, since at pH 4 all the fluorides are released from the DEX molecules.

Furthermore, the match between the kinetic trends of Cl^- and NH_4^+ ions, Fig. 1i supports the breakdown and complete mineralization of MTLC in the mixtures.

The previous results allow to conclude that complete mineralization of the organohalogen compounds and their intermediates has been achieved although it needs considerably longer times that the degradation of the primary compounds. As result of the photocatalytic treatment, no detectable organic carbon remains in the aqueous medium, which is substituted by the presence of halogen ions and ammonium. In this work, the concentrations of the latter, which depend on the initial concentration of OHXs, are found to be well below the levels permitted in drinking water by the World Health Organization (WHO) [65–67]. The guideline value for fluoride in drinking water, the most restrictive ion in this work, is 10 mg L^{-1}, thus discarding any potential health and environmental risk associated with the discharge of the treated waters.

3.3. *Catalyst performance*

The performance of the TiO_2/rGO photocatalyst has been evaluated by carrying out five consecutive cycles of 480 min each, determining the mineralization of the binary mixture DEX + MTLC, Fig. 3a, and the release of halogen ions, F^- and Cl^-, Fig. 3b. After 5 reusability runs, more than 80 % of the initial mass of TiO_2/rGO is recovered.

The adsorption capacity of MTLC on the catalyst surface does not change with the cycles ≈20 % of initial MTLC concentration is adsorbed in each run. Each cycle is followed along 480 min, and complete degradation of both MTLC and DEX is confirmed. Table 3 collects the

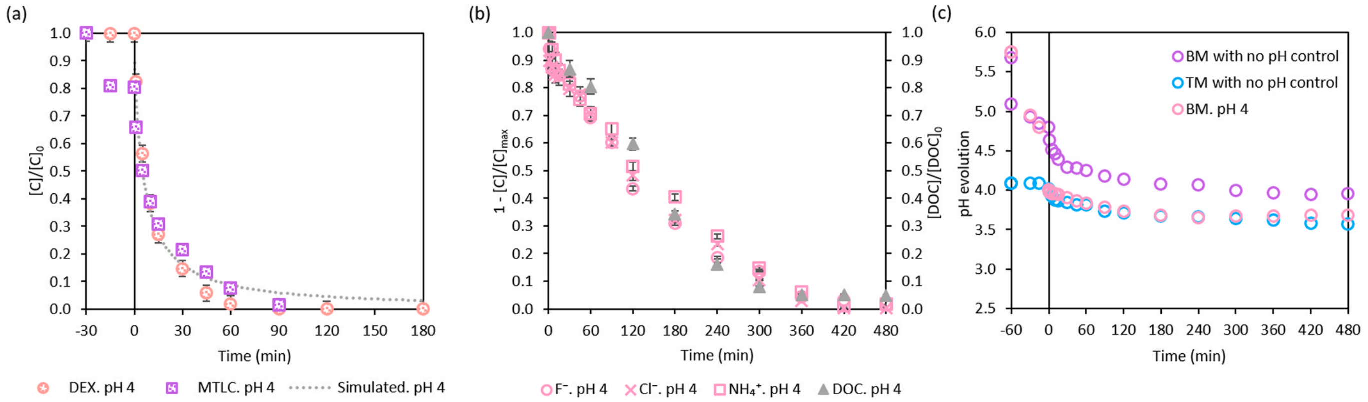

Fig. 2. (a) Photocatalytic degradation and (b) mineralization and ions released expressed as 1 - the dimensionless measured concentration in binary mixtures at pH 4, and (c) pH data corresponding to OHXs mixtures. BM: binary mixture. TM: tertiary mixture.

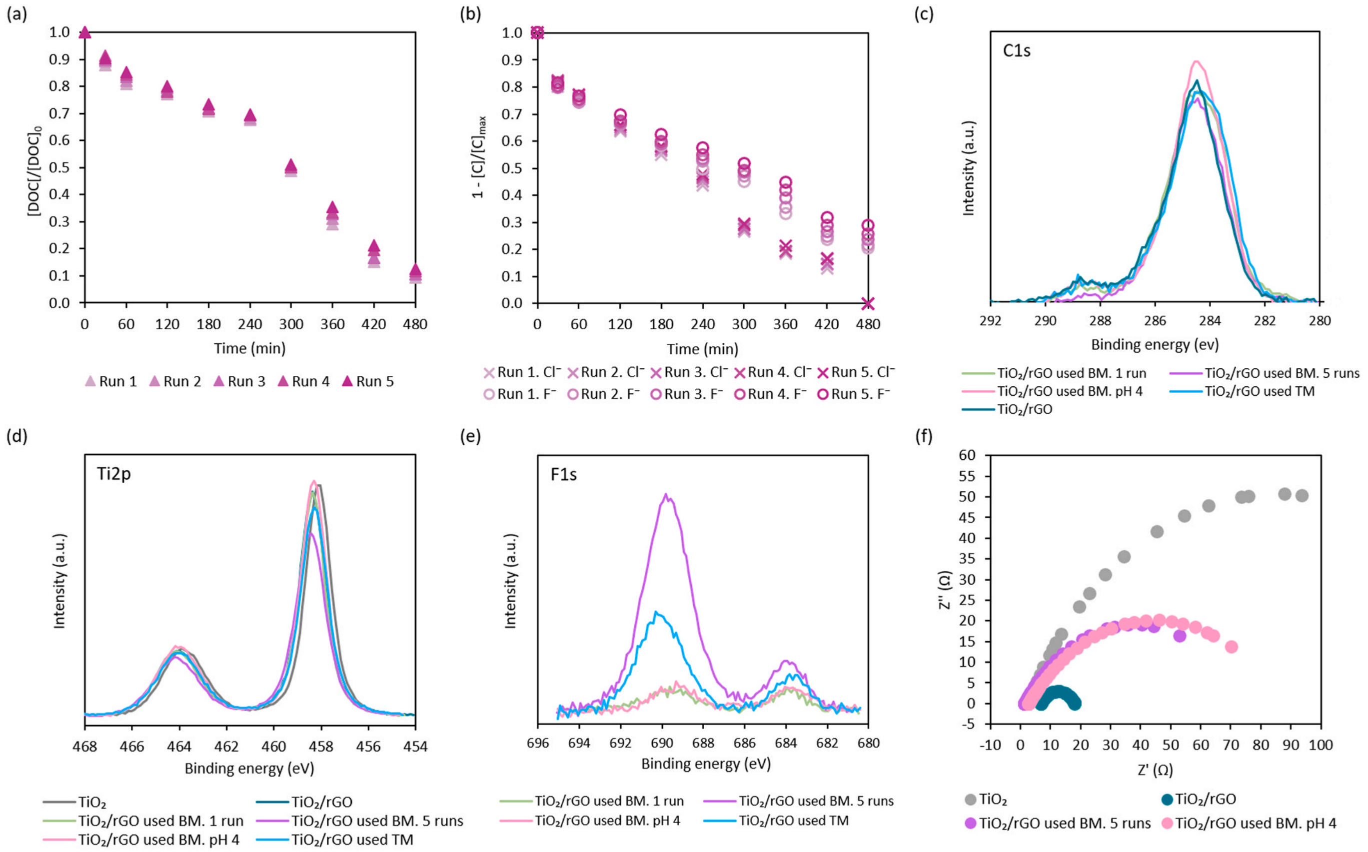

Fig. 3. TiO_2/rGO reusability studies for the binary mixture of DEX + MTLC with no pH control: (a) mineralization and (b) halogen released expressed as 1 - the dimensionless measured concentration. XPS high-resolution: (c) C1s, (d) Ti2p and (e) F1s spectra of the TiO_2/rGO used in the different mixtures. (f) Nyquist plot for the TiO_2/rGO bare and used in the different experiments. BM: binary mixture. TM: tertiary mixture.

values of the kinetic constants of mineralization and halogen ions release in the different cycles.

The consecutive photocatalytic runs have been performed with the recovered catalyst from the previous experiment. Therefore, to account for the loss of mass and the difference in the initial concentration of photocatalyst, a performance factor is included in Table 3, defined as the ratio between the kinetic constant and the initial catalyst concentration in each cycle. As evidenced in Table 3, the performance factor remains constant throughout the five photocatalytic cycles, with a slight reduction in the values corresponding to the rate of halogen release from the intermediate derivatives. This is attributed to the partial adsorption of fluoride on the photocatalyst surface. To support this information structural, XPS, Fig. 3c-e, electrochemical, EIS, Fig. 3f and morphological measurements, TEM, Fig. 4, are performed to the catalyst samples after different treatment sequences.

Fig. 3 displays XPS spectra corresponding to C1s (c), Ti2p (d) and F1s (e) of the different samples. In Fig. 3c the C1s spectra are depicted. In all samples, the peak with a binding energy (BE) of 284.3 eV can be attributed to the C-C, C═C, and C-H bonds [68,69]. The presence of these bonds is attributed to the reduced graphene oxide of the catalyst. Specially, the C═C bond is responsible for improving the conductivity of the catalyst, which is important for the efficient electron transfer [70, 71]. Regarding Ti2p spectra, Fig. 3d, there are two main peaks located at 458.35 eV and 464.10, attributed to $Ti2p_{3/2}$ and $Ti2p_{1/2}$, respectively. In addition, the splitting between both peaks is 5.75 eV, which indicates a Ti(IV) chemical state, typical of TiO_2 in GO-TiO_2 composites [72,73]. Ti2p spectrum corresponds to the TiO_2 commercial sample, showing symmetric components $2p_{3/2}$ and $2p_{1/2}$ [74]. It is noteworthy that no changes are observed in the titanium dioxide or reduced graphene oxide structures when analysing the results of used and fresh materials; this indicates that the photocatalyst retains its electronic structure. Finally, in Fig. 3e the spectra region of F1s is depicted confirming the presence of F in the catalyst after use in different runs. In all samples, two peaks are observed in the F1s spectra, located at 690 eV and 684 eV, confirming the presence of fluoride adsorbed on the materials that can be related to metal fluorides [75–77]. The TiO_2/rGO catalysts used in the binary mixtures after one run exhibited low intensity peaks. The intensity of the peaks increase in the catalyst used with the tertiary mixture and especially in the catalyst after five consecutive runs, indicating the accumulation of F on the material. These findings, firstly, point to the material balance between the adsorbed and solubilized fluoride in the reusability experiments, and are also related to the loss in the performance factor.

Furthermore, electrochemical impedance measurements have been carried out with the fresh and used composites as displayed in Fig. 3f. For comparative purposes, bare commercial TiO_2 P25 is included in Fig. 3f. The Nyquist plot of the commercial TiO_2 exhibits a resistance value, R_p, of 167.75 Ω whereas the TiO_2/rGO composite incorporating 5 % GO in its structure exhibits a resistance value of 11.84 Ω. The smaller resistance observed in the composite may indicate an improved electron excitation, efficient electron-hole separation, and enhanced electron transfer [56,78–81], confirming the advantages of using the composite with graphene over bare TiO_2. Then, when analysing the results of the used materials, similar values are displayed for the resistance of the catalyst used in the binary mixture after five runs and in the binary mixture at pH 4 after one run, $R_p \approx 78$ Ω, in agreement with the stability proved in the analysis of mineralization. In this work, the increased resistance can be attributed to the adsorbed fluoride on the catalyst surface, which blocks the active centers of the photocatalyst and worsens the electron movement.

Table 3
Kinetic constants for five consecutive cycles performed with the binary mixture DEX + MTLC with no pH control.

		Mineralization				Halogen release			
Run	TiO_2/ rGO ($g\ L^{-1}$)	First zone (0–240 min) Second order k ($mM^{-1}\ min^{-1}$)	Performance factor ($L\ mM^{-1}\ min^{-1}\ g^{-1}$)	Second zone (240–480 min) First order k (min^{-1})	Performance factor ($L\ min^{-1}\ g^{-1}$)	First zone (0–240 min) Second order k ($mM^{-1}\ min^{-1}$)	Performance factor ($L\ mM^{-1}\ min^{-1}\ g^{-1}$)	Second zone (240–480 min) First order k (min^{-1})	Performance factor ($L\ min^{-1}\ g^{-1}$)
1	0.50	0.58×10^{-3}	1.16×10^{-3}	7.30×10^{-3}	14.6×10^{-3}	43.8×10^{-3}	87.6×10^{-3}	5.71×10^{-3}	11.4×10^{-3}
2	0.48	0.56×10^{-3}	1.16×10^{-3}	6.94×10^{-3}	14.5×10^{-3}	42.1×10^{-3}	87.7×10^{-3}	5.59×10^{-3}	11.6×10^{-3}
3	0.46	0.53×10^{-3}	1.15×10^{-3}	6.91×10^{-3}	15.0×10^{-3}	40.9×10^{-3}	88.9×10^{-3}	5.14×10^{-3}	11.2×10^{-3}
4	0.44	0.51×10^{-3}	1.16×10^{-3}	6.54×10^{-3}	14.8×10^{-3}	39.3×10^{-3}	89.3×10^{-3}	4.69×10^{-3}	10.7×10^{-3}
5	0.42	0.49×10^{-3}	1.16×10^{-3}	6.20×10^{-3}	14.8×10^{-3}	36.9×10^{-3}	87.9×10^{-3}	4.32×10^{-3}	10.3×10^{-3}

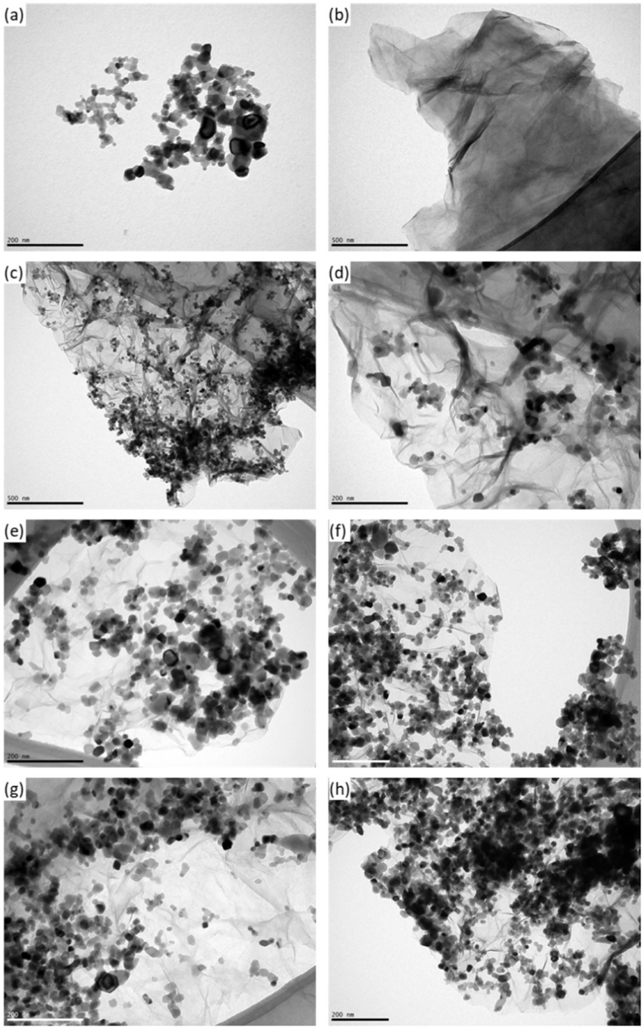

Fig. 4. TEM images of (a) TiO_2 P25, (b) rGO, (c,d) TiO_2/rGO fresh, (e) TiO_2/rGO used in the binary mixture after 1 cycle, (f) TiO_2/rGO used in the binary mixture after 5 cycles, (g) TiO_2/rGO used in the binary mixture at pH 4, 1 cycle, and (h) TiO_2/rGO used in the tertiary mixture.

In Fig. 4a, bare TiO_2 is arranged in spherical shaped particles with an average diameter of 20 nm, which is characteristic of titanium dioxide P25 [82,83]. Fig. 4b exhibits pure rGO with a crumpled two-dimensional structure with a wavy morphology [84–86]. Fig. 4c and Fig. 4d show TEM images of TiO_2/rGO at two different magnifications. Both images show round TiO_2 particles clustered on a rGO sheet, demonstrating the success of the TiO_2 particle surface decoration during the hydrothermal synthesis, which increases the active surface area [87]. TiO_2 particles appear to be distributed in an uneven manner on the rGO sheets, particularly over the edges and folds [88,89]. Fig. 4e-h shows TEM images of the TiO_2/rGO photocatalyst used after different experiments. In terms of shape, it is found that all the used catalyst samples retain their morphology. When used, TiO_2 particles remain perfectly anchored to the rGO films, with the same particle size as in the fresh composite.

BET analysis has been carried out to determine the specific surface area. Table S1 in the SM summarises the BET surface area values for the fresh TiO_2 P25, TiO_2/rGO, and the composites used with different mixtures. The BET surface area of commercial TiO_2 P25 is ≈50 $m^2\ g^{-1}$, which is consistent with the reported values in literature [90,91]. The incorporation of rGO into bare TiO_2 results in an increase in the BET surface area by 35 %, with a value of 65.7 ± 2.8 $m^2\ g^{-1}$. These findings are in accordance with those of Wang et al. (2012) [92], who observed an increase in the specific surface area as the rGO content in various TiO_2/rGO photocatalysts was increased. Moreover, BET surface area values of the materials used in the binary and tertiary mixtures exhibit a change of less than 10 % in comparison to fresh TiO_2/rGO, concluding the stability of this parameter with the catalyst use.

3.4. *Phytotoxicity assessment*

Together with the analysis of the degree of carbon removal, assessment of the toxicity is essential for water remediation processes, as the reaction intermediates and final products may become more hazardous than the initial OHXs [93,94]. The literature typically recognizes as the absence of phytotoxic substances if GI ≥ 80 % and GI ≤ 50 % is regarded as highly toxic and not suitable for water reuse as agricultural purposes [61]. Thereby, phytotoxicity tests have been performed using the specie Sorghum saccharatum (SOS). Fig. 5 collects the germination indices (GI) of the (a) roots and (b) shoots of the seeds during five reusability experiments of the binary mixture DEX + MTLC, as well as the GI of the control sample (20 mL of ultrapure water, as recommended by the technical data sheet). The mean GI for all the experimental times (excluding the control) is indicated by the dashed lines in Fig. 5 with roots and shoots values of 79 %, and 74 %, respectively. Consequently, it can be inferred that the average GI value is close to the value that is typically recognized in the literature as the absence of phytotoxic substances (GI ≥ 80 %) for both roots and shoots.

As seen in Fig. 5, all runs maintain the same evolution, with standard deviation errors lower than 10 %. GI values obtained for the initial samples (without treatment) of the roots and shoots of the binary mixture before treatment are 46 % and 43 %, respectively. As the photocatalytic reactions progress, the root and shoot GI values approach the 80 % value until they finally overpass it. Regarding the roots and shoots, Fig. 5a, and Fig. 5b, GI values ≥ 80 % are reached in approximately 240 min of UV-A irradiation, which means that even if in that moment the initial OHXs are totally degraded, the intermediate compounds formed during photocatalytic treatment add toxicity to the aqueous medium; this highlights once more the relevance of undertaking

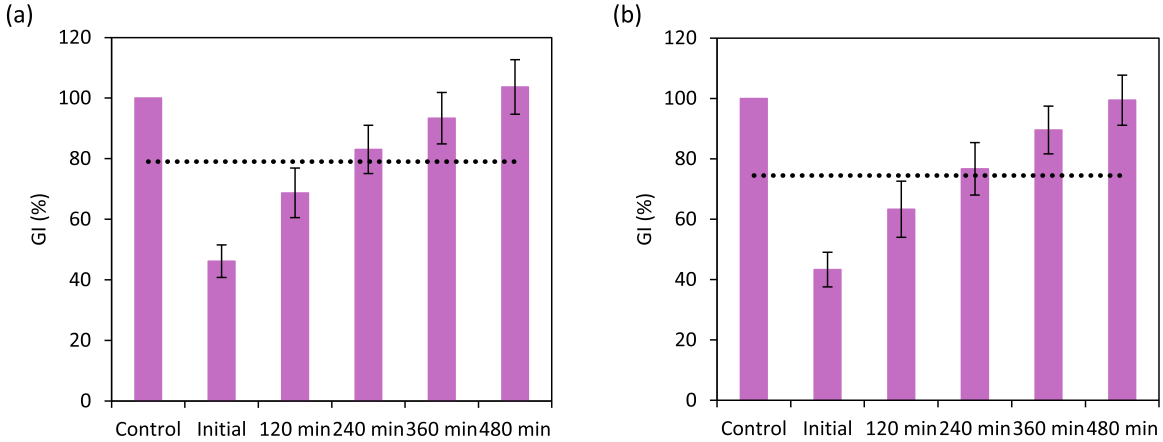

Fig. 5. Germination index obtained with Sorghum saccharatum seeds for (a) roots, and (b) shoots throughout the five experiments of TiO_2/rGO reuse in the binary mixture DEX + MTLC degradation with no pH control. The dashed horizontal lines represent the average of all samples (excluding the control).

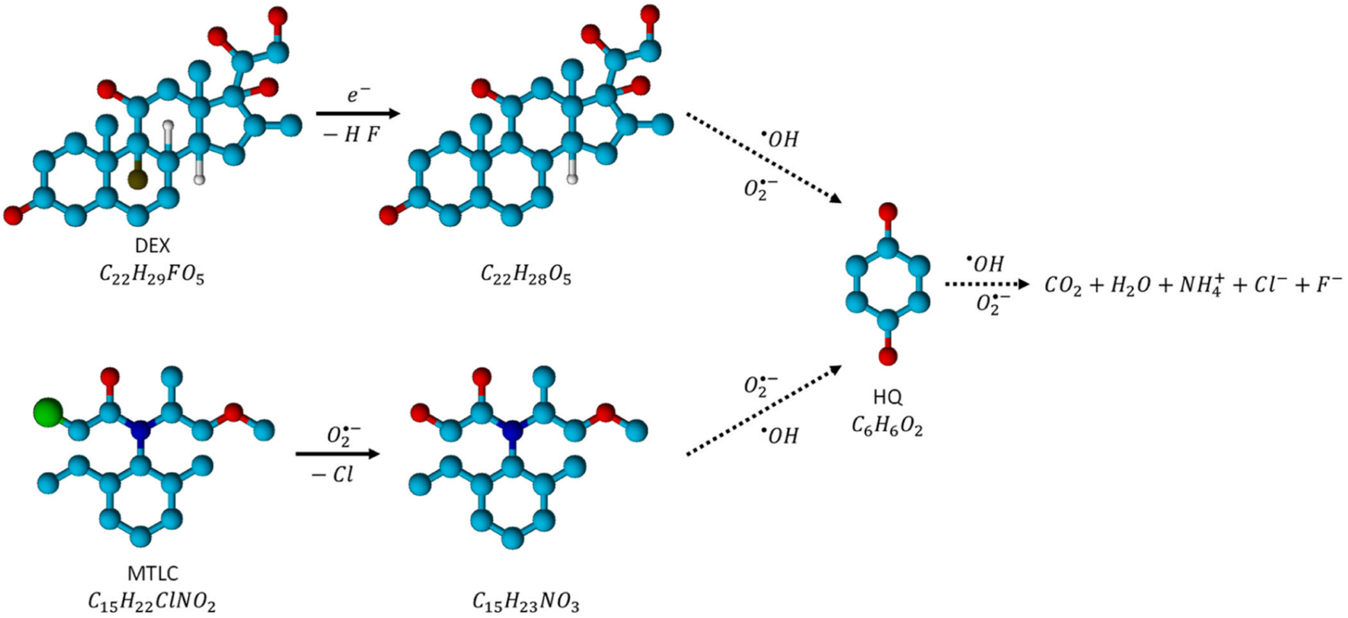

Fig. 6. Tentative mechanism of DEX and MTLC dehalogenation, HQ formation and mineralization. The solid line represents dehalogenation by a direct reaction. The dashed line represents the formation of HQ, CO_2 and H_2O by intermediate reactions. (Representation drawn using the ChemDraw online server).

conditions of full mineralization to support the green and sustainable character of photocatalysis. The inflection point around 240 min also corresponds to the period when mineralization starts to be faster, indicating that the more recalcitrant and more toxic by-products probably start degrading from this point onwards. GI values only exceed the control point after 360 min of experimentation, that is time enough for complete mineralization. On average, the final root and shoot GI values after 480 minutes of treatment are 103 %, and 99 %, respectively. To sum up, for times of complete mineralization the photocatalytically treated medium does not present phytotoxicity.

The quantification of the mineralization kinetics, together with the assessment of no residual toxicity, is the first and necessary step prior to process design and optimization. Apart from the improved performance of TiO_2/rGO composites, other variables that have influence on the treatment time must be considered in a real application, such as the influence of the light source, the correct optimization and design of the photocatalytic reactor, etc., is justified over the commercial TiO_2 due to the improved kinetic constants, which favors considerably the design and process optimization. Furthermore, the use of UV-A LEDs results in a significant saving of electrical energy [95–97].

Fig. 6 presents a simplified mechanism that encompasses the dehalogenation of DEX and MTLC [58], through the formation of hydroquinone (HQ) from both molecules, and the final products of complete mineralization. For DEX, it is common for the C-F bond to be broken in the first stage of its photodegradation. DEX loses the fluorine atom by reductive dehalogenation. In the case of MTLC, dechlorination occurs by displacement of chloride by a nucleophilic superoxide radical [58]. In this work, we identify HQ as intermediate product from both DEX and MTLC molecules. HQ formation is a consequence of the attack of hydroxyl and superoxide radicals to the aromatic ring [98]. Further information is included in the supplementary material.

4. Conclusions

A holistic methodology that combines monitoring of environmental and phytotoxicity parameters in the aqueous medium over time with changes in the morphological and structural characteristics of the photocatalyst has been applied to the photocatalytic treatment of aqueous solutions containing three organohalogen compounds of great concern; the selected OHXs belonging to the groups of pharmaceuticals, DEX containing 1 F atom, herbicides, MTLC containing 1 Cl atom and disinfection byproducts, DCA containing 2 Cl atoms, have been photocatalytically treated with a low-cost and easily synthesizable TiO_2/rGO composite. A detailed experimental plan has allowed us to identify the main variables that affect the catalyst performance, confirming the beneficial impact of the acidic media; the obtained kinetic parameters are essential for the correct design and optimization of the process. In the field of water remediation, the analysis of the performance of new catalytic materials must go beyond their activity in the degradation of primary compounds and include the monitoring of global parameters, such as dissolved organic carbon and the toxicity of the treated water, which require longer operation times and depend on operating conditions. This work advances the existing knowledge in the photocatalytic mineralization of mixtures of OHXs with TiO_2/rGO as photocatalyst, and highlights the relevance of properly analyze the kinetics of degradation, mineralization and release of ions into the aqueous medium. To make photocatalysis more competitive compared to conventional water remediation technologies, future work should focus on the development of kinetic models that detail the influence of the variables of the liquid medium and of the solid, to continue with the design and process optimization.

CRediT authorship contribution statement

María J Rivero: Writing – review & editing, Validation, Supervision, Resources, Project administration, Methodology, Funding acquisition, Conceptualization. **Inmaculada Ortiz:** Writing – review & editing, Validation, Supervision, Resources, Methodology, Funding acquisition, Conceptualization. **Carmen Barquín:** Writing – review & editing, Writing – original draft, Validation, Methodology, Investigation, Formal analysis, Conceptualization.

Declaration of Competing Interest

The authors declare that they have no known competing financial interests or personal relationships that could have appeared to influence the work reported in this paper.

Acknowledgements

These results are part of the R&D projects PID2021-122563OB-I00 funded by MICIU/AEI/10.13039/501100011033 and by "ERDF/EU", and PDC2022-133563-I00, funded by MICIU/AEI/10.13039/501100011033 and by the "European Union NextGenerationEU/PRTR". Carmen Barquín is also grateful for the grant PRE2019-089096 funded by MICIU/AEI/10.13039/501100011033 and by "ESF Investing in your future". The authors would like to thank the DEPRO group of the Universidad de Cantabria an in particular José Antonio Abarca for his invaluable help with the impedance measurements. Also, the authors acknowledge the SERMET of the Universidad de Cantabria for TEM measurements. We would also like to extend our gratitude to the research group of Professor José Rodríguez Mirasol at the Universidad de Málaga for their contributions to the XPS measurements.

Appendix A. Supporting information

Supplementary data associated with this article can be found in the online version at doi:10.1016/j.jece.2024.114572.

Data availability

The data that has been used are confidential.

References

[1] S.K. Fanourakis, J. Peña-Bahamonde, P.C. Bandara, D.F. Rodrigues, Nano-based adsorbent and photocatalyst use for pharmaceutical contaminant removal during indirect potable water reuse, NPJ Clean. Water 3 (2020), https://doi.org/10.1038/s41545-019-0048-8.

[2] A. Hernández-Zanoletty, O. Cabezuelo, A. Parı́s-Reche, I. Oller, M.I. Polo-López, A. Agüera, P. Plaza, M.L. Marı́n, F. Boscá, S. Malato, Assessment of new immobilized photocatalysts based on TiO_2 for wastewater decontamination, J. Environ. Chem. Eng. 11 (2023), https://doi.org/10.1016/j.jece.2023.111291.

[3] S.A. Bhat, V. Kumar, F. Li, P. Verma, Detection and Treatment of Emerging Contaminants in Wastewater, IWA Publishing, 2024, https://doi.org/10.2166/9781789063752.

[4] R. Yin, L. Ling, S. Lu, H. Li, C. Li, C. Shang, Degradation of aliphatic halogenated contaminants in water by UVA/Cu–TiO_2 and UVA/TiO_2 photocatalytic processes: structure-activity relationship and role of reactive species, Chemosphere 260 (2020) 127644, https://doi.org/10.1016/j.chemosphere.2020.127644.

[5] M.J. Rivero, P. Ribao, B. Gomez-Ruiz, A. Urtiaga, I. Ortiz, Comparative performance of TiO_2-rGO photocatalyst in the degradation of dichloroacetic and perfluorooctanoic acids, Sep. Purif. Technol. 240 (2020) 116637, https://doi.org/10.1016/j.seppur.2020.116637.

[6] M. Ren, P. Zhao, X. Fu, M. Liu, Y. Ning, Y. Zhang, C. Wang, A. Lin, J. Cui, Phase-modulated built-in electric field to boost photogenerated electron migration for efficient dehalogenation, Chem. Eng. J. 474 (2023) 145524, https://doi.org/10.1016/j.cej.2023.145524.

[7] D.E. Lee, M.K. Kim, M. Danish, W.K. Jo, State-of-the-art review on photocatalysis for efficient wastewater treatment: attractive approach in photocatalyst design and parameters affecting the photocatalytic degradation, Catal. Commun. 183 (2023) 106764, https://doi.org/10.1016/j.catcom.2023.106764.

[8] M. Ahtasham Iqbal, S. Akram, S. khalid, B. Lal, S.U. Hassan, R. Ashraf, G. Kezembayeva, M. Mushtaq, N. Chinibayeva, A. Hosseini-Bandegharaei, Advanced photocatalysis as a viable and sustainable wastewater treatment process: a comprehensive review, Environ. Res. 253 (2024) 118947, https://doi.org/10.1016/j.envres.2024.118947.

[9] A. Singh, J. Dhau, R. Kumar, R. Badru, P. Singh, Y. Kumar Mishra, A. Kaushik, Tailored carbon materials (TCM) for enhancing photocatalytic degradation of polyaromatic hydrocarbons, Prog. Mater. Sci. 144 (2024) 101289, https://doi.org/10.1016/j.pmatsci.2024.101289.

[10] J.O. Adeyemi, T. Ajiboye, D.C. Onwudiwe, Mineralization of antibiotics in wastewater via photocatalysis, Water Air. Soil Pollut. 232 (2021) 1–28, https://doi.org/10.1007/s11270-021-05167-3.

[11] L. Belhacova, T. Supinkova, A. Panacek, L. Hochvaldova, R. Prucek, R. Zouzelka, J. Rathousky, The role of TiO_2 photocatalyst in degradation of halogenated phenols: experimental, DFT and antibacterial study, Appl. Catal. A Gen. 656 (2023) 119134, https://doi.org/10.1016/j.apcata.2023.119134.

[12] X. Chen, Y. Li, X. Pan, D. Cortie, X. Huang, Z. Yi, Photocatalytic oxidation of methane over silver decorated zinc oxide nanocatalysts, Nat. Commun. 7 (2016) 1–8, https://doi.org/10.1038/ncomms12273.

[13] L. Moura, R.C. Picão, Removal of Antimicrobial Resistance Determinants from Wastewater: A Risk Perspective on Conventional and Emerging Technologies. in: Emerg. Contam. Environ., Elsevier, 2022, pp. 603–642, https://doi.org/10.1016/B978-0-323-85160-2.00023-8.

[14] Q. Guo, C. Zhou, Z. Ma, X. Yang, Fundamentals of TiO_2 photocatalysis: concepts, mechanisms, and challenges, Adv. Mater. 31 (2019) 1–26, https://doi.org/10.1002/adma.201901997.

[15] S.K. Loeb, P.J.J. Alvarez, J.A. Brame, E.L. Cates, W. Choi, J. Crittenden, D. D. Dionysiou, Q. Li, G. Li-Puma, X. Quan, D.L. Sedlak, T. David Waite, P. Westerhoff, J.H. Kim, The technology horizon for photocatalytic water treatment: sunrise or sunset? Environ. Sci. Technol. 53 (2019) 2937–2947, https://doi.org/10.1021/acs.est.8b05041.

[16] X. Chen, S.S. Mao, Titanium dioxide nanomaterials: synthesis and applications, Chem. Rev. 107 (2007) 2821–3361, https://doi.org/10.14233/ajchem.2023.27287.

[17] T. Hirakawa, Y. Nosaka, Properties of $O2^{\cdot -}$ and $OH^{\cdot}$ formed in TiO_2 aqueous suspensions by photocatalytic reaction and the influence of H_2O_2 and some ions, Langmuir 18 (2002) 3247–3254, https://doi.org/10.1021/la015685a.

[18] Y. Nam, J.H. Lim, K.C. Ko, J.Y. Lee, Photocatalytic activity of TiO_2 nanoparticles: a theoretical aspect, J. Mater. Chem. A. 7 (2019) 13833–13859, https://doi.org/10.1039/c9ta03385h.

[19] S.M. Gupta, M. Tripathi, A review of TiO_2 nanoparticles, Chin. Sci. Bull. 56 (2011) 1639–1657, https://doi.org/10.1007/s11434-011-4476-1.

[20] G. Žerjav, Z. Say, J. Zavašnik, M. Finšgar, C. Langhammer, A. Pintar, Photo, thermal and photothermal activity of TiO_2 supported Pt catalysts for plasmon-driven environmental applications, J. Environ. Chem. Eng. 11 (2023), https://doi.org/10.1016/j.jece.2023.110209.

[21] H. Zhang, Y. Xiao, Z. Zhang, J. Han, Z. Wu, Z. Wei, Y. Zhu, Q. Guo, L. Tian, Y. Tang, Simultaneous removal of CTRX and Cr(VI) by CQDs-doped bifunctional molecular imprinted BiOCl/Bi_3NbO_7 photocatalyst: the enhanced selective performance and charge separation abilities, J. Environ. Chem. Eng. 12 (2024) 113597, https://doi.org/10.1016/j.jece.2024.113597.

[22] W. Zhao, J. Li, T. She, S. Ma, Z. Cheng, G. Wang, P. Zhao, W. Wei, D. Xia, D.Y. C. Leung, Study on the photocatalysis mechanism of the Z-scheme cobalt oxide nanocubes/carbon nitride nanosheets heterojunction photocatalyst with high photocatalytic performances, J. Hazard. Mater. 402 (2021) 123839, https://doi.org/10.1016/j.jhazmat.2020.123839.

[23] T. Xu, S. Wang, T. Wang, X. Li, Y. Chen, Q. Wu, L. Yang, X. Liu, M. Wei, J. Cao, Boosting electron transfer by coupling Ag NPs and direct Z-scheme heterojunction in Fe_3O_4@SiO_2@ZnO-pda-Ag for enhanced photocatalysis, Mater. Sci. Semicond. Process. 179 (2024) 108535, https://doi.org/10.1016/j.mssp.2024.108535.

[24] X. Zhang, X. Gu, Y. Song, R. Xie, S. Zhang, J. Li, S. Sheng, H. Zou, One-step synthesis of oxygen vacancy-rich BiOBr/TiO_2 composite: ultrafast adsorption-photocatalytic performance and mechanism, Chem. Eng. J. 495 (2024) 153261, https://doi.org/10.1016/j.cej.2024.153261.

[25] S. Nazari, E. Asgari, A. Sheikhmohammadi, S.A. Mokhtari, H. Alamgholiloo, Visible-light-driven photocatalytic activity of WO_3/ZIF-67 S-scheme heterojunction for upgrading degradation of oxytetracycline, J. Environ. Chem. Eng. 11 (2023) 110393, https://doi.org/10.1016/j.jece.2023.110393.

[26] Y. Zhang, C. Liang, K. Zhang, Y. Zeng, Y. Zhou, X. Zhang, L. Yin, J. Crittenden, J. Niu, Tandem photocatalysis of nitrate to nitrogen on Cu@CN/TiO_x S-scheme heterojunction, Sep. Purif. Technol. 348 (2024) 127686, https://doi.org/10.1016/j.seppur.2024.127686.

[27] H. Mittal, M. Khanuja, Nanosheets- and nanourchins-like nanostructures of $MoSe_2$ for photocatalytic water purification: kinetics and reusability study, Environ. Sci. Pollut. Res. 27 (2020) 23477–23489, https://doi.org/10.1007/s11356-019-06275-8.

[28] D. Danilian, F.M. Bundrück, A. Kikas, T. Käämbre, H. Mändar, S. Lehner, A. Gogos, J. Kozlova, M. Kook, V. Kiisk, J. Link, R. Stern, A. Ivask, V. Kisand, R. Pärna, Reusable magnetic mixture of $CuFe_2O_4$-Fe_2O_3 and TiO_2 for photocatalytic degradation of pesticides in water, RSC Adv. 14 (2024) 12337–12348, https://doi.org/10.1039/d4ra00094c.

[29] O. Oyegbeda, S.O. Akpotu, B. Moodley, A novel Z-scheme covalent triazine framework/silver phosphate (CTF/Ag_3PO_4) heterojunction photocatalyst: improved adsorption, photocatalytic degradation and degradation mechanism of rifampicin, J. Environ. Chem. Eng. 12 (2024) 113447, https://doi.org/10.1016/j.jece.2024.113447.

[30] X. Jiang, L. Huang, J. Li, L. Zhang, X. Guo, Y. Li, X. Sun, A novel strategy to construct the superior performance of 3D multi-shell CeO_2/ZnO@ZnS as a reusable sunlight-driven ternary photocatalyst for highly efficient water remediation, J. Environ. Chem. Eng. 9 (2021) 105608, https://doi.org/10.1016/j.jece.2021.105608.

[31] N. Madima, K.K. Kefeni, A.T. Kuvarega, S.B. Mishra, A.K. Mishra, Visible-light-driven Z-scheme ternary Fe_3O_4/TiO_2/g-C_3N_4 nanocomposite as reusable photocatalyst for efficient removal of dyes and chromium in water, Mater. Chem. Phys. 296 (2023) 127233, https://doi.org/10.1016/j.matchemphys.2022.127233.

[32] M. Huang, J. Xiong, X. Xiao, Z. Jiang, Y. Liang, Y. Cai, Y. Zeng, Y. Chen, $BiOIO_3$/$Bi_{12}SiO_{20}$ core-shell S-type heterojunction for efficient photocatalytic removal of bisphenol A: performance and mechanism study, J. Environ. Chem. Eng. 12 (2024) 113455, https://doi.org/10.1016/j.jece.2024.113455.

[33] M.A. Abbasi, K.M. Amin, M. Ali, Z. Ali, M. Atif, W. Ensinger, W. Khalid, Synergetic effect of adsorption-photocatalysis by GO−CeO_2 nanocomposites for photodegradation of doxorubicin, J. Environ. Chem. Eng. 10 (2022), https://doi.org/10.1016/j.jece.2021.107078.

[34] Z. Huang, P. Zhu, S. Zhang, M. Duan, M. Liu, X. Li, Synthesis of double Z-type heterojunction AgI/$Ag_6Si_2O_7$/BiOI photocatalyst for antibiotics degradation and weakening toxicity, J. Environ. Chem. Eng. 12 (2024) 113432, https://doi.org/10.1016/j.jece.2024.113432.

[35] A. Shawky, R.M. Mohamed, S-scheme heterojunctions: emerging designed photocatalysts toward green energy and environmental remediation redox reactions, J. Environ. Chem. Eng. 10 (2022) 108249, https://doi.org/10.1016/j.jece.2022.108249.

[36] J.H. Shen, T.H. Chiang, C.K. Tsai, Z.W. Jiang, J.J. Horng, Mechanistic insights into hydroxyl radical formation of Cu-doped ZnO/g-C_3N_4 composite photocatalysis for enhanced degradation of ciprofloxacin under visible light: efficiency, kinetics, products identification and toxicity evaluation, J. Environ. Chem. Eng. 10 (2022) 107352, https://doi.org/10.1016/j.jece.2022.107352.

[37] N.C. Chiu, J.M. Lessard, E.N. Musa, L.S. Lancaster, C. Wheeler, T.D. Krueger, C. Chen, T.C. Gallagher, M.T. Nord, H. Huang, P.H.Y. Cheong, C. Fang, K. C. Stylianou, Elucidation of the role of metals in the adsorption and photodegradation of herbicides by metal-organic frameworks, Nat. Commun. 15 (2024) 1–12, https://doi.org/10.1038/s41467-024-45546-y.

[38] B. Wang, Y. Chen, J. Samba, K. Heck, X. Huang, J. Lee, J. Metz, M. Bhati, J. Fortner, Q. Li, P. Westerhoff, P. Alvarez, T.P. Senftle, M.S. Wong, Surface hydrophobicity of boron nitride promotes PFOA photocatalytic degradation, Chem. Eng. J. 483 (2024) 149134, https://doi.org/10.1016/j.cej.2024.149134.

[39] B. Castanheira, L. Otubo, C.L.P. Oliveira, R. Montes, J.B. Quintana, R. Rodil, S. Brochsztain, V.J.P. Vilar, A.C.S.C. Teixeira, Functionalized mesoporous silicas SBA-15 for heterogeneous photocatalysis towards CECs removal from secondary urban wastewater, Chemosphere 287 (2022), https://doi.org/10.1016/j.chemosphere.2021.132023.

[40] J. Bockenstedt, N.A. Vidwans, T. Gentry, S. Vaddiraju, Catalyst recovery, regeneration and reuse during large-scale disinfection of water using photocatalysis, Water 13 (2021), https://doi.org/10.3390/w13192623.

[41] S.A. Younis, K.H. Kim, Heterogeneous photocatalysis scalability for environmental remediation: opportunities and challenges, Catalysts 10 (2020) 1–8, https://doi.org/10.3390/catal10101109.

[42] Y. Li, Y. Ma, K. Li, S. Chen, D. Yue, Photocatalytic reactor as a bridge to link the commercialization of photocatalyst in water and air purification, Catalysts 12 (2022), https://doi.org/10.3390/catal12070724.

[43] E.H. Khader, T.J. Mohammed, T.M. Albayati, H.N. Harharah, A. Amari, N.M. C. Saady, S. Zendehboudi, Current trends for wastewater treatment technologies with typical configurations of photocatalytic membrane reactor hybrid systems: a review, Chem. Eng. Process. Process. Intensif. 192 (2023) 109503, https://doi.org/10.1016/j.cep.2023.109503.

[44] K.H. Hama Aziz, F.S. Mustafa, K.M. Omer, I. Shafiq, Recent advances in water falling film reactor designs for the removal of organic pollutants by advanced oxidation processes: a review, Water Resour. Ind. 30 (2023) 100227, https://doi.org/10.1016/j.wri.2023.100227.

[45] P. Kumari, N. Bahadur, L.F. Dumée, Photo-catalytic membrane reactors for the remediation of persistent organic pollutants – a review, Sep. Purif. Technol. 230 (2020) 115878, https://doi.org/10.1016/j.seppur.2019.115878.

[46] S. Karoui, A.A. Assadi, A. Ghorbal, L. Khezami, A. Assadi, S. Loganathan, A. Amrane, Enhancement of water remediation by innovative photocatalytic luminous textiles reactor: performance, kinetic modeling, and mechanistic insights, J. Water Process Eng. 56 (2023) 104448, https://doi.org/10.1016/j.jwpe.2023.104448.

[47] J.A. Rengifo-Herrera, C. Pulgarin, Why five decades of massive research on heterogeneous photocatalysis, especially on TiO_2, has not yet driven to water disinfection and detoxification applications? Critical review of drawbacks and challenges, Chem. Eng. J. 477 (2023), https://doi.org/10.1016/j.cej.2023.146875.

[48] Z. Kuspanov, B. Bakbolat, A. Baimenov, A. Issadykov, M. Yeleuov, C. Daulbayev, Photocatalysts for a sustainable future: innovations in large-scale environmental and energy applications, Sci. Total Environ. 885 (2023) 163914, https://doi.org/10.1016/j.scitotenv.2023.163914.

[49] A.A. Ioannidi, O.S. Arvaniti, K. Miserli, I. Konstantinou, Z. Frontistis, D. Mantzavinos, Removal of drug dexamethasone from aqueous matrices using low frequency ultrasound: kinetics, transformation products, and effect of microplastics, J. Environ. Manag. 328 (2023) 117007, https://doi.org/10.1016/j.jenvman.2022.117007.

[50] A.V. Quaresma, K.T.S. Rubio, J.G. Taylor, B.A. Sousa, S.Q. Silva, A.A. Werle, R.J.C. F. Afonso, Removal of dexamethasone by oxidative processes: structural characterization of degradation products and estimation of the toxicity, J. Environ. Chem. Eng. 9 (2021) 106884, https://doi.org/10.1016/j.jece.2021.106884.

[51] V.A. Sakkas, I.M. Arabatzis, I.K. Konstantinou, A.D. Dimou, T.A. Albanis, P. Falaras, Metolachlor photocatalytic degradation using TiO_2 photocatalysts, Appl. Catal. B Environ. 49 (2004) 195, https://doi.org/10.1016/j.apcatb.2003.12.008.

[52] C.A. Orge, M.F.R. Pereira, J.L. Faria, Photocatalytic-assisted ozone degradation of metolachlor aqueous solution, Chem. Eng. J. 318 (2017) 247, https://doi.org/10.1016/j.cej.2016.06.136.

[53] A. Šuligoj, M. Kete, U. Černigoj, F. Fresno, U. Lavrenčič Štangar, Synergism in TiO_2 photocatalytic ozonation for the removal of dichloroacetic acid and thiacloprid, Environ. Res. 197 (2021), https://doi.org/10.1016/j.envres.2021.110982.

[54] G. Cavallo, P. Metrangolo, R. Milani, T. Pilati, A. Priimagi, G. Resnati, G. Terraneo, The halogen bond, Chem. Rev. 116 (2016) 2478–2601, https://doi.org/10.1021/acs.chemrev.5b00484.

[55] C. Barquín, M.J. Rivero, I. Ortiz, Shedding light on the performance of magnetically recoverable TiO_2/Fe_3O_4/rGO-5 photocatalyst. Degradation of S-metolachlor as case study, Chemosphere 307 (2022) 135991, https://doi.org/10.1016/j.chemosphere.2022.135991.

[56] J.A. Abarca, I. Merino-Garcia, G. Díaz-Sainz, M. Perfecto-Irigaray, G. Beobide, A. Irabien, J. Albo, Fabrication and optimization of perovskite-based photoanodes for solar-driven CO_2 photoelectroreduction to formate, Catal. Today 429 (2024), https://doi.org/10.1016/j.cattod.2023.114505.

[57] S. Castro, J. Albo, A. Irabien, Continuous conversion of CO_2 to alcohols in a TiO_2 photoanode-driven photoelectrochemical system, J. Chem. Technol. Biotechnol. 95 (2020) 1876–1882, https://doi.org/10.1002/jctb.6315.

[58] C. Barquín, M.J. Rivero, I. Ortiz, Photodegradation kinetics and halogens release of the emerging concern pollutants dexamethasone and S-metolachlor on TiO_2/rGO composites, Chemosphere 349 (2024) 140806, https://doi.org/10.1016/j.chemosphere.2023.140806.

[59] B. Gómez-Ruiz, P. Ribao, N. Diban, M.J. Rivero, I. Ortiz, A. Urtiaga, Photocatalytic degradation and mineralization of perfluorooctanoic acid (PFOA) using a composite TiO_2−rGO catalyst, J. Hazard. Mater. 344 (2018) 950–957, https://doi.org/10.1016/j.jhazmat.2017.11.048.

[60] L. Rancaño, M.J. Rivero, M.Á. Mueses, I. Ortiz, Comprehensive kinetics of the photocatalytic degradation of emerging pollutants in a led-assisted photoreactor. S-metolachlor as case study, Catalysts 11 (2021) 1–13, https://doi.org/10.3390/catal11010048.

[61] J.A.F. Batista, J. Mendes, W.E. Moretto, M.S. Quadro, J.H.Z. dos Santos, C.C. de Escobar, Sunlight removal of diclofenac using g-C_3N_4, g-C_3N_4/Cl, g-C_3N_4/Nb_2O_5 and g-C_3N_4/TiO_2 photocatalysts, J. Environ. Chem. Eng. 12 (2024), https://doi.org/10.1016/j.jece.2024.113016.

[62] P. Ribao, M.J. Rivero, I. Ortiz, Enhanced photocatalytic activity using GO/TiO_2 catalyst for the removal of DCA solutions, Environ. Sci. Pollut. Res. 25 (2018) 34893, https://doi.org/10.1007/s11356-017-0901-6.

[63] D.R.Vieira Guelfi, F. Gozzi, A. Machulek, I. Sirés, E. Brillas, S.C. de Oliveira, Degradation of herbicide S-metolachlor by electrochemical AOPs using a boron-doped diamond anode, Catal. Today 313 (2018) 182–188, https://doi.org/10.1016/j.cattod.2017.10.026.

[64] Y. Chen, Q. Chen, R.M. Kasomo, Y. Jin, P. Yang, H. Zheng, X. Weng, H. Li, S. Song, Adsorption of fluoride from aqueous solutions using graphene oxide composite materials at a neutral pH, J. Mol. Liq. 377 (2023) 121467, https://doi.org/10.1016/j.molliq.2023.121467.

[65] World Health Organization (WHO), Fluoride in Drinking-water, in: WHO Guidel. Drink. Qual., 2004.

[66] World Health Organization (WHO), Chloride in Drinking-water, in: WHO Guidel. Drink. Qual., 2003.

[67] World Health Organization (WHO), Ammonia in Drinking-water, in: WHO Guidel. Drink. Qual., 2003.

[68] F. Wang, K. Zhang, Reduced graphene oxide-TiO_2 nanocomposite with high photocatalystic activity for the degradation of rhodamine B, J. Mol. Catal. A Chem. 345 (2011) 101–107, https://doi.org/10.1016/j.molcata.2011.05.026.

[69] P. Wang, J. Wang, X. Wang, H. Yu, J. Yu, M. Lei, Y. Wang, One-step synthesis of easy-recycling TiO_2-rGO nanocomposite photocatalysts with enhanced photocatalytic activity, Appl. Catal. B Environ. 132-133 (2013) 452–459, https://doi.org/10.1016/j.apcatb.2012.12.009.

[70] H. Fan, G. Yi, X. Zhang, B. Xing, C. Zhang, L. Chen, Y. Zhang, Facile synthesis of uniformly loaded Fe_3O_4–TiO_2/RGO ternary hybrids for enhanced photocatalytic activities, Opt. Mater. 111 (2021) 110582, https://doi.org/10.1016/j.optmat.2020.110582.

[71] W. Lin, X. Xie, X. Wang, Y. Wang, D. Segets, J. Sun, Efficient adsorption and sustainable degradation of gaseous acetaldehyde and o-xylene using rGO-TiO_2 photocatalyst, Chem. Eng. J. 349 (2018) 708–718, https://doi.org/10.1016/j.cej.2018.05.107.

[72] P. Benjwal, M. Kumar, P. Chamoli, K.K. Kar, Enhanced photocatalytic degradation of methylene blue and adsorption of arsenic(III) by reduced graphene oxide (rGO)-metal oxide (TiO_2/Fe_3O_4) based nanocomposites, RSC Adv. 5 (2015) 73249, https://doi.org/10.1039/c5ra13689j.

[73] L.M. Pastrana-Martínez, S. Morales-Torres, V. Likodimos, J.L. Figueiredo, J. L. Faria, P. Falaras, A.M.T. Silva, Advanced nanostructured photocatalysts based on reduced graphene oxide-TiO_2 composites for degradation of diphenhydramine pharmaceutical and methyl orange dye, Appl. Catal. B Environ. 123–124 (2012) 241–256, https://doi.org/10.1016/j.apcatb.2012.04.045.

[74] ThermoScientific Knowledge Database, Titanium, (2022). ⟨https://www.jp.xpssimplified.com/elements/titanium.php⟩ (accessed February 23, 2022).

[75] ThermoFisher Scientific, XPS Halogen Fluorine, (2024). ⟨https://srdata.nist.gov/xps/⟩ (accessed May 27, 2024).

[76] National Institute of Standards and Technology (NIST), X-ray Photoelectron Spectroscopy Database, (2024). ⟨https://www.thermofisher.com/es/es/home/materials-science/learning-center/periodic-table/halogen/fluorine.html⟩ (accessed May 27, 2024).

[77] E. McCafferty, J.P. Wightman, Determination of the concentration of surface hydroxyl groups on metal oxide films by a quantitative XPS method, Surf. Interface Anal. 26 (1998) 549, https://doi.org/10.1002/(sici)1096-9918(199807)26:8<549::aid-sia396>3.3.co;2-h.

[78] Y. Li, C. Lou, W. Huang, Z. Ma, S. Lin, X. Xie, T. He, X. Lu, N. Chen, J. Zhuang, MoO_2-C@MoS_2: a unique cocatalyst with LSPR effect for enhanced quasi-full-spectrum photocatalytic hydrogen evolution of CdS, Appl. Catal. B Environ. 343 (2024) 123543, https://doi.org/10.1016/j.apcatb.2023.123543.

[79] E.A. AbdulKareem, Z.H. Mahmoud, A.A. Khadom, Sunlight assisted photocatalytic mineralization of organic pollutants over rGO impregnated TiO_2 nanocomposite: theoretical and experimental study, Case Stud. Chem. Environ. Eng. 8 (2023) 100446, https://doi.org/10.1016/j.cscee.2023.100446.

[80] A. Tolosana-Moranchel, J.A. Casas, A. Bahamonde, L. Pascual, L.I. Granone, J. Schneider, R. Dillert, D.W. Bahnemann, Nature and photoreactivity of TiO_2-rGO nanocomposites in aqueous suspensions under UV-A irradiation, Appl. Catal. B Environ. 241 (2019) 375–384, https://doi.org/10.1016/j.apcatb.2018.09.070.

[81] N.T. Padmanabhan, N. Thomas, J. Louis, D.T. Mathew, P. Ganguly, H. John, S. C. Pillai, Graphene coupled TiO_2 photocatalysts for environmental applications: a review, Chemosphere 271 (2021) 129506, https://doi.org/10.1016/j.chemosphere.2020.129506.

[82] S. Rajendran, A. Blanco, L. Gnanasekaran, A.A. Jalil, W.H. Chen, F. Gracia, Harvesting visible light for enhanced catalytic degradation of wastewater using TiO_2@Fe_3O_4 embedded on two dimensional reduced graphene oxide nanosheets, Chemosphere 345 (2023) 140418, https://doi.org/10.1016/j.chemosphere.2023.140418.

[83] T. Ohno, K. Sarukawa, K. Tokieda, M. Matsumura, Morphology of a TiO_2 photocatalyst (Degussa, P-25) consisting of anatase and rutile crystalline phases, J. Catal. 203 (2001) 82–86, https://doi.org/10.1006/jcat.2001.3316.

[84] N.P. Rajkumari, S. Dolakashoria, P. Goswami, Plant-based natural dye-stimulated visible-light reduction of GO and physicochemical factors influencing the production of oxidizing species by a synthesized (rGO)/TiO_2 nanocomposite for environmental remediation, ACS Omega 6 (2021) 2686–2698, https://doi.org/10.1021/acsomega.0c04889.

[85] M. Utami, S. Wang, M.M. Musawwa, T.E. Purbaningtias, M. Fitri, I. Yuspita, O. H. Abd-Elkader, K.K. Yadav, G. Munusamy-Ramanujam, D. Bang, S.W. Chang, B. Ravindran, Simultaneous photocatalytic removal of organic dye and heavy metal from textile wastewater over N-doped TiO_2 on reduced graphene oxide, Chemosphere 332 (2023) 138882, https://doi.org/10.1016/j.chemosphere.2023.138882.

[86] H.M. Moustafa, M. Obaid, M.M. Nassar, M.A. Abdelkareem, M.S. Mahmoud, Titanium dioxide-decorated rGO as an effective electrode for ultrahigh-performance capacitive deionization, Sep. Purif. Technol. 235 (2020) 116178, https://doi.org/10.1016/j.seppur.2019.116178.

[87] R. Rashid, I. Shafiq, M.R.H.S. Gilani, M. Maaz, P. Akhter, M. Hussain, K.E. Jeong, E. E. Kwon, S. Bae, Y.K. Park, Advancements in TiO_2-based photocatalysis for environmental remediation: strategies for enhancing visible-light-driven activity, Chemosphere 349 (2024) 140703, https://doi.org/10.1016/j.chemosphere.2023.140703.

[88] D.M. Tobaldi, D. Dvoranová, L. Lajaunie, N. Rozman, B. Figueiredo, M.P. Seabra, A.S. Škapin, J.J. Calvino, V. Brezová, J.A. Labrincha, Graphene-TiO_2 hybrids for photocatalytic aided removal of VOCs and nitrogen oxides from outdoor environment, Chem. Eng. J. 405 (2021), https://doi.org/10.1016/j.cej.2020.126651.

[89] A. Ojha, P. Singh, R. Oraon, D. Tiwary, A.K. Mishra, A.A. Ghfar, M. Naushad, T. Ahamad, B. Thokchom, K. Vijayaraghavan, S. Rangabhashiyam, An environmental approach for the photodegradation of toxic pollutants from wastewater using silver nanoparticles decorated titania-reduced graphene oxide, J. Environ. Chem. Eng. 9 (2021) 105622, https://doi.org/10.1016/j.jece.2021.105622.

[90] C.H. Chiou, C.Y. Wu, R.S. Juang, Influence of operating parameters on photocatalytic degradation of phenol in UV/TiO_2 process, Chem. Eng. J. 139 (2008) 322–329, https://doi.org/10.1016/j.cej.2007.08.002.

[91] H. Znad, K. Abbas, S. Hena, M.R. Awual, Synthesis a novel multilamellar mesoporous TiO_2/ZSM-5 for photo-catalytic degradation of methyl orange dye in aqueous media, J. Environ. Chem. Eng. 6 (2018) 218–227, https://doi.org/10.1016/j.jece.2017.11.077.

[92] D. Wang, X. Li, J. Chen, X. Tao, Enhanced photoelectrocatalytic activity of reduced graphene oxide/TiO_2 composite films for dye degradation, Chem. Eng. J. 198–199 (2012) 547–554, https://doi.org/10.1016/j.cej.2012.04.062.

[93] A.L. Garcia-Costa, T.I.A. Gouveia, M.F.R. Pereira, A.M.T. Silva, L.M. Madeira, A. Alves, M.S.F. Santos, Intensification strategies for cytostatics degradation by ozone-based processes in aqueous phase, J. Hazard. Mater. 440 (2022), https://doi.org/10.1016/j.jhazmat.2022.129743.

[94] J.A. Zazo, J.A. Casas, C.B. Molina, A. Quintanilla, J.J. Rodriguez, Evolution of ecotoxicity upon Fenton's oxidation of phenol in water, Environ. Sci. Technol. 41 (2007) 7164–7170, https://doi.org/10.1021/es071063l.

[95] F. Ahmad, M. Mehmood, A critical review of photocatalytic degradation of organophosphorus pesticide “Parathion” by different mixed metal oxides, Adv. J. Chem. Sect. A. 5 (2022) 287–310, https://doi.org/10.22034/ajca.2022.357664.1324.

[96] A. Serrà, L. Philippe, F. Perreault, S. Garcia-Segura, Photocatalytic treatment of natural waters. Reality or hype? The case of cyanotoxins remediation, Water Res. 188 (2021), https://doi.org/10.1016/j.watres.2020.116543.

[97] D. Wang, A.L. Junker, M. Sillanpää, Y. Jiang, Z. Wei, Photo-based advanced oxidation processes for zero pollution: where are we now? Engineering 23 (2023) 19–23, https://doi.org/10.1016/j.eng.2022.08.005.

[98] M. Pazoki, M. Parsa, R. Farhadpour, Removal of the hormones dexamethasone (DXM) by Ag doped on TiO_2 photocatalysis, J. Environ. Chem. Eng. 4 (2016) 4426–4434, https://doi.org/10.1016/j.jece.2016.09.034.